IEEE Access
Multidisciplinary | Rapid Review | Open Access Journal

Received June 25, 2018, accepted July 26, 2018, date of publication August 6, 2018, date of current version September 5, 2018.

Digital Object Identifier 10.1109/ACCESS.2018.2862626

Structure Tensor Graph Searches Based Fully Automated Grading and 3D Profiling of Maculopathy From Retinal OCT Images

TAIMUR HASSAN[1], MUHAMMAD USMAN AKRAM[1], (Member, IEEE), ARSLAN SHAUKAT[1], SAJID GUL KHAWAJA[1], AND BILAL HASSAN[2]

[1]Department of Computer and Software Engineering, National University of Sciences and Technology, Islamabad 44000, Pakistan
[2]School of Automation Science and Electrical Engineering, Beihang University, Beijing 100191, China

Corresponding author: Taimur Hassan (engr.taimoorhassan@gmail.com)

This work was supported by the Ignite National Technology Fund, Government of Pakistan.

ABSTRACT Maculopathy is a collective group of diseases that damages the central region of a retina known as macula. The major two forms of maculopathy are macular edema (ME) and central serous chorioretinopathy (CSCR). Different researchers have worked on the identification of these macular disorders using optical coherence tomography (OCT) images. However, to the best of our knowledge, no research is reported until now that can automatically extract retinal information for the grading of ME and CSCR as per clinically significant ME (CSME), non-clinically significant ME (non-CSME), Type-I CSCR, and Type-II CSCR clinical standards from OCT images. Therefore, this paper presents a novel structure tensor graph searches (ST-GS)-based segmentation framework that combines a structure tensor and graph theory to automatically extract retinal and choroidal layers along with fluid pores followed by automated reconstruction of 3-D retinal surfaces. The ST-GS can extract retinal information even from highly degraded OCT scans. Furthermore, the proposed system automatically grades ME and CSCR pathologies as CSME and non-CSME and Type-I CSCR and Type-II CSCR, respectively. The proposed system extracts seven distinct features, and it is trained on 30 (10 healthy, 10 ME, and 10 CSCR) labeled OCT volumes containing 3840 brightness scans (B-scans). After that, 90 (30 healthy, 30 CSCR, and 30 ME) unlabeled OCT volumes containing 11520 B-scans were used for testing the proposed system, where it correctly classified 88 out of 90 cases with the sensitivity, specificity, and accuracy ratings of 96.77%, 100%, and 97.78%, respectively. Furthermore, the proposed system has achieved a mean dice coefficient of 0.875 ± 0.0342 and 0.92 ± 0.0258 for extracting cyst and serous fluids, respectively.

INDEX TERMS Biomedical image processing, image analysis, optical coherence tomography, ophthalmology, pattern recognition.

I. INTRODUCTION

Human retina mainly consists of two regions i.e. the macular and the ocular region. Macular region is where the vision is formed. Maculopathy tends to damage the macular region resulting in vision loss or even blindness. The two major macular syndromes are macular edema (ME) and central serous chorioretinopathy (CSCR), also known as central serous retinopathy (CSR). ME is mainly found in diabetic patients, where the retinal blood vessels become thinned because of hyperglycemia and leak proteins or other fluid deposits within retinal layers. CSCR is caused due to leakage of serous within retinal pigment epithelium (RPE) layer. In case of CSCR, the neurosensory retina remains in contact while it is distorted in case of ME. ME is clinically graded into two stages depending upon the severity of retinal thickness as defined by the study of early treatment diabetic retinopathy (ETDRS) [1]. Edema within the diameter of 500 micrometers centered at fovea is considered to be severe, because it significantly causes vision loss or blindness. This stage is termed as clinically significant macular edema (CSME). The retinal edema outside this limit is known as non-clinically significant macular edema (non-CSME). CSCR is also graded into two stages. Usually serous accumulates under the neurosensory retina and this type of condition leads to Type I CSCR. CSCR due to serous formation beneath RPE [2] is known as Type II CSCR. Figure 1 depicts healthy, CSCR and ME

2169-3536 © 2018 IEEE. Translations and content mining are permitted for academic research only.
Personal use is also permitted, but republication/redistribution requires IEEE permission.
See http://www.ieee.org/publications_standards/publications/rights/index.html for more information.

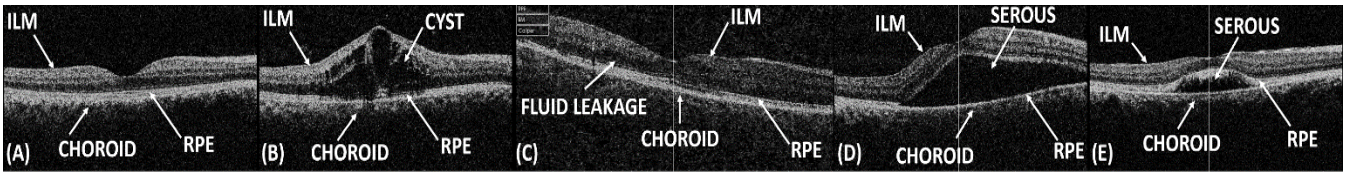

FIGURE 1. Retinal OCT images: (A) normal brightness scan (B-scan), (B) CSME B-scan, (C) non-CSME B-scan, (D) Type-I CSCR B-scan, (E) Type-II CSCR B-scan.

affected retinal OCT scans along with different severity levels. Maculopathy can be identified through different testing techniques. The most commonly used techniques are fundography, fundus fluorescein angiography (FFA) and OCT. FFA is the best technique to visualize macular pathology, however it is invasive and many people are allergic to the dye that is injected in the vein. OCT is the recently introduced technique that can objectively detect early syndromes of macular and ocular disorders. OCT is based on Michelson interferometer principle [3] and the major advantage of OCT over other techniques is that it can detect early symptoms of maculopathy. Different researchers have presented their findings about ME and CSCR from OCT scans. Hannouche *et al.* [4] assessed fundography, bio-microscopy, FFA and OCT to detect diabetic foveal edema. They concluded that OCT can give objective evaluation about the severity of maculopathy as compared to other techniques. Zhang *et al.* [5] proposed the use of OCT in the early treatment of diabetic macular edema (DME). Shrestha *et al.* [6] proposed the effective usage of OCT imaging in aligning the macula after ME surgery. Their study involved 60 patients. Mokwa *et al.* [7] drew a comparison between OCT imaging technique, FFA and fundus photography (FP) for detecting exudative and non-exudative macular degeneration. They concluded that FP best indicates the RPE changes and drusen in case of age related macular degeneration (AMD). However, OCT is more sensitive in detecting minor changes in case of CNV. Helmy *et al.* [8] proposed classification of cystoid macular edema (CME) based on OCT findings in 104 eyes of 86 patients. They concluded that OCT provides better characterization of CME, and hence is very useful technique in quantitative measurement. Ferrara *et al.* [9] identified the distinctive features of RPE and choroid that appears in OCT scans of patients suffering from CSCR. They considered 15 eyes of 13 patients in their study. Wani *et al.* [10] diagnosed CSCR from 48 eyes and concluded that OCT is an effective technique that can be used as a complement to FFA for the detection of CSCR. Teke *et al.* [11] compared FFA and OCT for evaluating the abnormalities in 100 CSCR patients and concluded that both techniques can help and back the clinicians to detect CSCR. Ahlers *et al.* [12] discussed the alteration in the retinal layers of CSCR affected OCT scans. They studied 18 subjects of CSCR and concluded that OCT imaging is more useful as it provides exact information regarding morphological changes along with retinal microstructure. Mitarai *et al.* [13] found the changes at leakage points in CSCR affected OCT scans. They included 26 subjects in their study out of which 23 were men and 3 were women, and concluded that OCT noninvasively detects the morphologic alteration with much ease in case of CSCR.

Some researchers have automatically detected ME using OCT images. Wilkins *et al.* [14] identified the retinal fluid by annotating ILM and RPE and have evaluated their system on the dataset consisting of 16 eye patients. They achieved the average specificity of 96% and mean sensitivity of 91% for detecting retinal fluid. Sugruk *et al.* [15] proposed an automated method for classifying diabetic macular edema (DME) and AMD subjects. For classifying DME subjects, they have extracted cyst segments with accuracy of 86.6% while for detecting AMD, they clipped nerve fiber layer (NFL) from OCT scans to extract RPE and achieved an accuracy of 100% for AMD subjects. Zhang *et al.* [16] extracted retinal layers for the diagnosis of cystoid macular edema (CME) through adaptive boosting. Their achieved accuracy was 98.6%. Srinivasan *et al.* [17] proposed a fully automated SVM based method to detect DME, AMD and healthy subjects from retinal OCT scans. The accuracy of their proposed system was 100% for AMD cases, 100% for DME cases and 86.67% for healthy cases respectively. Recently Rashno *et al.* [18] proposed a fully automated neutrosophic transformation and graph based shortest path method to segment cyst regions from DME affected OCT scans. However, to the best of our knowledge there is no technical paper available that can automatically grade ME into CSME, non-CSME and CSCR into Type-I CSCR and Type-II CSCR from OCT images.

Previously we have proposed automated systems in [19]–[22] to diagnose ME, CSCR and AMD from OCT volumes. However, the proposed system is an upgraded version of our previous work [19]–[22] with the significant new contributions. In [19], we presented an automated system for the diagnosis of ME and CSR subjects through reconstruction of 3D retinal surfaces. The method proposed in [19] was a 3D solution for the objective diagnosis of ME and CSR pathologies, however it lacks the ability to automatically grade ME and CSR subjects according to CSME, non-CSME, Type-I and Type-II clinical standards. In [20] and [21], we proposed an automated diagnostic system for screening healthy and maculopathy subjects from 2D OCT brightness scans (B-scans). The methods proposed in [20] and [21] only take 2D B-scans as input and therefore the diagnosis is based on single B-scan acquired from foveal location. The system

proposed in [21] utilized a structure tensor based segmentation framework for extracting retinal layers from CSR and ME pathologies. In [21] and [22], there were limitations of poor quality scans i.e. the retinal layer segmentation does not work well for poor quality images as already discussed in [21] and [22]. Furthermore, the system proposed in [22] only utilized retinal layers for diagnosing healthy and ME subjects, however the extraction and visualization of cyst fluid also indicate the major findings in diagnosing ME clinically which is missing in [22].

To summarize, the major contributions of this paper are:

- This paper presents a structure tensor graph searches (ST-GS) framework that combines tensors and graph theory to extract up to eight retinal and choroidal layers from OCT scans regardless of scan quality or the retinal pathology. ST-GS framework outperforms our original structure tensor based segmentation framework [20]–[22] by providing better layers segmentation even from highly degraded scans as shown in Figure 13.
- Apart from just diagnosing maculopathy, the proposed framework is first of its kind that can automatically measure the severity of the underlying disease and grades it accordingly as per CSME, non-CSME, Type-I CSCR and Type-II CSCR clinical standards.
- It is worth noting that the proposed system presents a highly detailed presentation of 3D retinal thickness surfaces which are further utilized in diagnosing maculopathy through hierarchical SVM based classification model.
- The proposed system achieved the sensitivity, specificity and accuracy ratings of 96.77%, 100% and 97.78% and a mean dice coefficient of 0.875±0.0342 and 0.92±0.0258 for extracting cyst and serous fluids respectively.

Rest of the paper is organized as follows: Section II explains the proposed system in detail, section III highlights the performance and results achieved by the proposed system in automatically grading macular subjects, section IV presents a detailed discussion about the proposed system along with its applications and section V outlines conclusions and future directions.

II. PROPOSED METHODOLOGY

The detailed block level diagram of proposed system is presented in Figure 2. At first, an input OCT volume is loaded

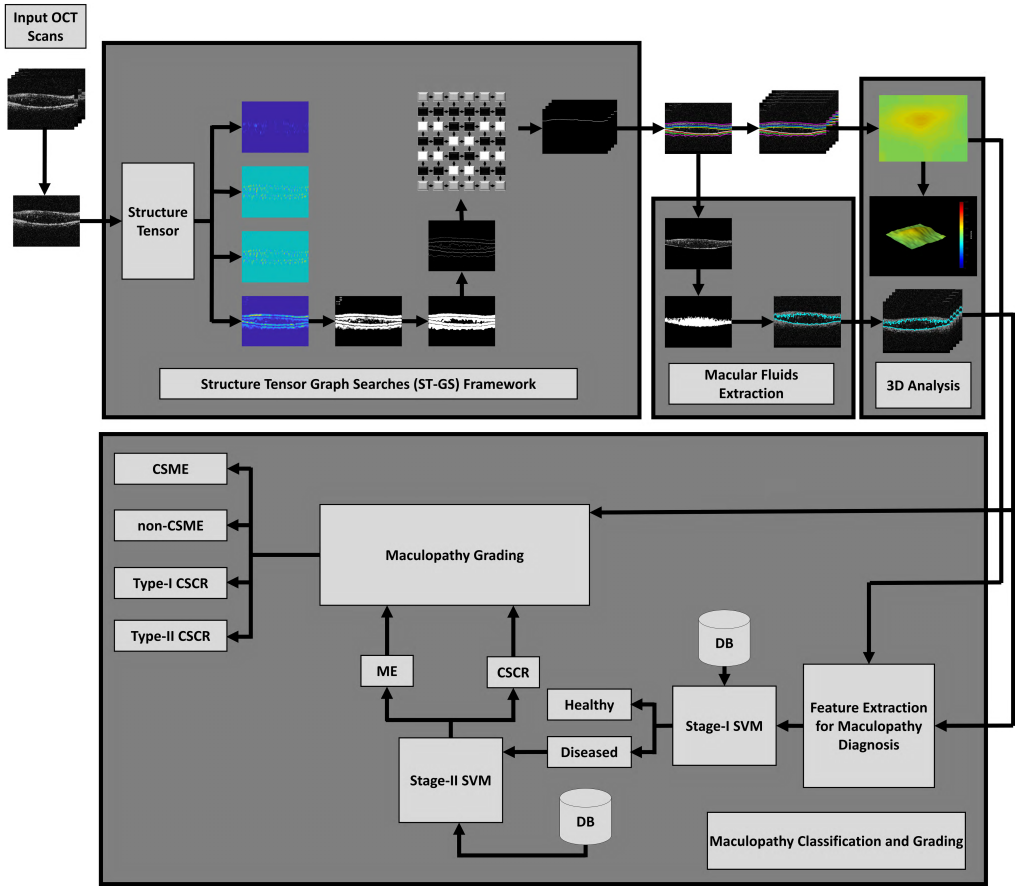

FIGURE 2. Proposed system. Each OCT scan within the volume is processed individually where retinal and choroidal layers are extracted first through proposed ST-GS framework. The fluids are extracted with the help of extracted ILM and RPE layers. The extracted retinal information is passed to the hierarchical SVM based classification model for the diagnosis and grading of maculopathy.

into the proposed system where each frame $F \in \mathbb{R}^{M\times N}$ (M denote the rows and N denote the columns of F) is processed individually. F is then passed to the structure tensor graph searches (ST-GS) framework from which the 2D structure tensor is extracted and then the highly coherent tensor is automatically selected by measuring the degree of coherency [20]–[22]. Afterwards, the coherent tensor is digitalized using 6 passes of hysteresis threshold and later on decomposed into an undirected graph from which the retinal and choroidal layers are automatically traced. After extracting the layers information, ILM and RPE are utilized in obtaining fluid regions by generating a binary mask which is multiplied with the original scan. Furthermore, ILM and RPE are also used to generate retinal thickness profiles in each B-scan to extract the thickness level of retina. This process is repeated for all the frames within OCT volume and the extracted thickness as well as fluid profiles are used to reconstruct 3D retinal surfaces and macular fluids. These surfaces are then utilized in obtaining discriminating feature-set to screen maculopathy subjects from normal ones and then to characterize maculopathy cases as ME or CSCR positive through hierarchical SVM based classification model. Furthermore, the proposed system automatically analyzes the severity of diagnosed maculopathy by extracting clinically significant features for each macular syndrome. To the best of our knowledge, this is the first ever framework that is able to grade the severity levels of ME and CSCR syndromes from OCT scans according to the clinical standards. Furthermore, the proposed system has been applied on 15,360 B-scans of different retinal pathologies, which clearly indicates the robustness of the proposed system.

A. OCT DATASET ACQUISITION

The dataset used in this research contains OCT volumes of 120 subjects in which 69 were male and 51 were female. There are 15,360 B-scans (3,840 B-scans for training and 11,520 B-scans for validation) within the dataset in which there are 5,120 healthy, 5,120 CSCR and 5,120 ME affected B-scans. The dataset has been acquired using TOPCON 3D OCT 3000 machine in Armed Forces Institute of Ophthalmology (AFIO), Rawalpindi and all the scans are labeled by multiple expert ophthalmologists. Apart from scan labeling, the expert ophthalmologists also annotated the retinal and choroidal layers as well as fluid segments based upon their experience in an isolated room. The detailed description about the dataset is tabulated in Table 1.

TABLE 1. Dataset description.

Parameters	Healthy	CSCR	ME
Frame resolution (pixel x pixel)	951 x 456	951 x 456	951 x 456
Axial scans (pixels)	951	951	951
B-scans in each volume	128	128	128
Total volumes	40	40	40
Graded volumes	-	Type-I: 31 Type-II: 9 Total: 40	CSME: 23 non-CSME: 17 Total: 40
Total B-scans	5,120	5,120	5,120
Acquired from	Armed Forces Institute of Ophthalmology (AFIO), Rawalpindi Pakistan		
Acquisition machine	TOPCON 3D OCT 3000		

B. STRUCTURE TENSOR GRAPH SEARCHES (ST-GS) FRAMEWORK

ST-GS is an improved version of original structure tensor based segmentation framework [20]–[22] which combines coherent tensors with state of the art graph theory for extracting up to eight retinal and choroidal layers regardless of the image quality or the retinal pathology. ST-GS works by computing coherent tensor of OCT B-scan F (x, y) within OCT volume V_{OCT}(x, y, z) and tracing each layer iteratively from the best selected tensor. The detailed explanation about structure tensor is already presented in [20]–[22] and here we are only focusing on the improvements which we made in the existing framework to generalize it for the extraction of retinal and choroidal layers from OCT images irrespective of the scan quality or retinal pathology. After extracting a coherent tensor, it is digitalized through 6 passes of hysteresis threshold. Hysteresis thresholding uses two thresholds t_l and t_h. If the pixel within an image is lower than t_l then the respective pixel in the resultant image is set to 0 and if the pixel is higher than t_h, then the respective pixel in the resultant image is set to 1. However, for those pixels which are in between t_l and t_h, their respective pixel in the resultant image is set to 1 if they are neighbors with the pixels which are greater than t_h. Afterwards, thick edges from the binarized tensor are adjusted through morphological skeletonization and the skeletonized scan is decomposed into an undirected graph, where each pixel corresponds to a node and adjacent nodes are connected to each other via 4-neighbor connectivity. ST-GS then automatically traces each layer iteratively. The tracing algorithm works in a way that it first generates binary map for each retinal layer and initializes the seed points within the graph. At each iteration, the seed points traverse to nearest node by measuring the intensity differences. If the intensity difference between two or more nodes is same, then top seed points give priority to downward nodes. Similarly, the bottom seed points give priority to upward nodes. When the top or bottom seed point observes a transition between foreground and background pixel, then they include that pixel into the respective layer map and change the foreground pixel to background. The whole algorithm converges when the initialized seed points becomes equal. The block diagram of the whole ST-GS framework is shown in Figure 3 for the randomly selected scan where τ_{XX}, τ_{XY}, τ_{YX} and τ_{YY} denotes the obtained tensors at respective orientations and i denotes the iteration of graph searches algorithm.

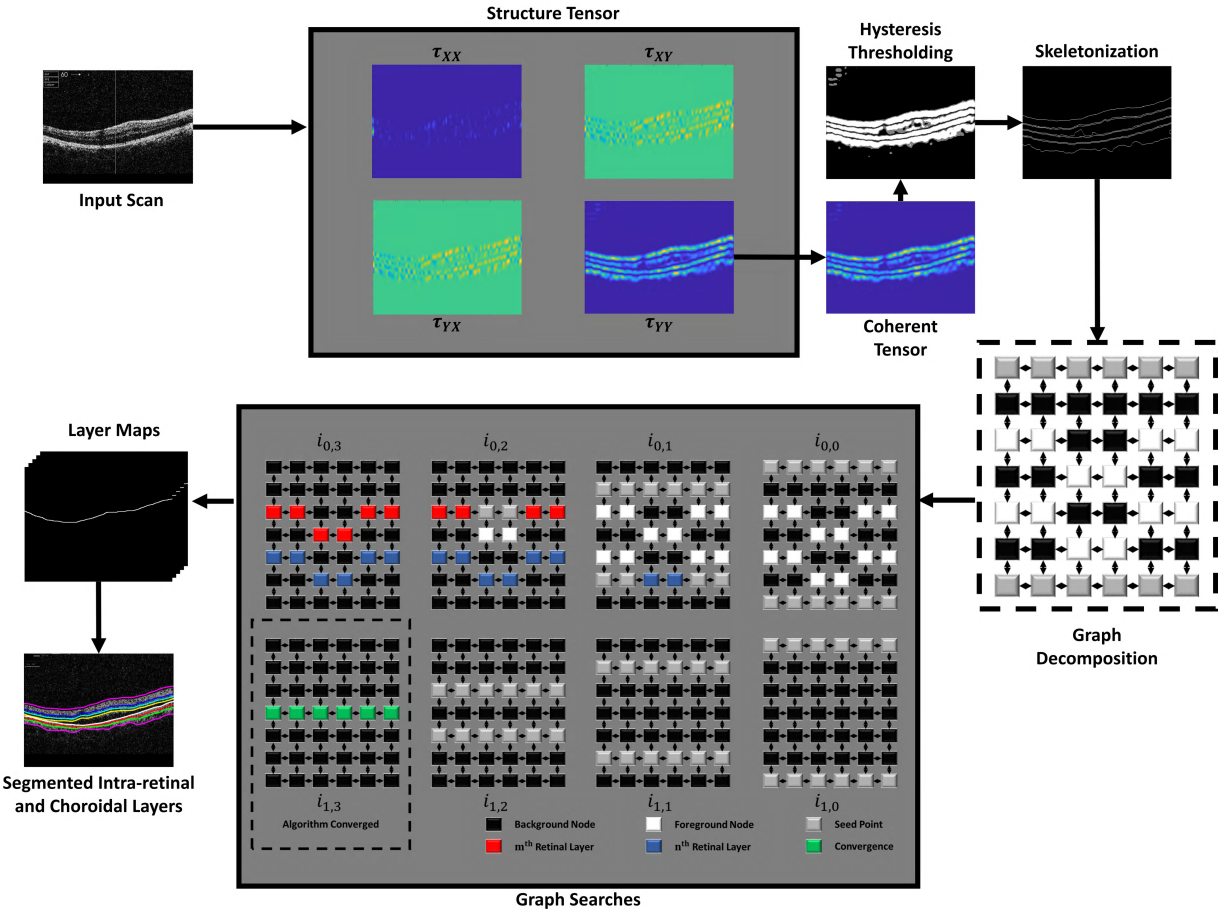

FIGURE 3. Proposed structure tensor graph searches (ST-GS) framework.

Retina comprises of various retinal layers such as ILM, retinal nerve fiber layer (RNFL), ganglion cell layer (GCL), inner plexiform layer (IPL), inner nuclear layer (INL), outer plexiform layer (OPL), outer nuclear layer (ONL), inner segment (IS), outer segment (OS), retinal pigment epithelium (RPE) and Bruch's membrane (BM). Beneath BM lies choroid. Retinal layers segmented from 3 randomly selected CSCR, healthy and ME cases are shown in Figure 4.

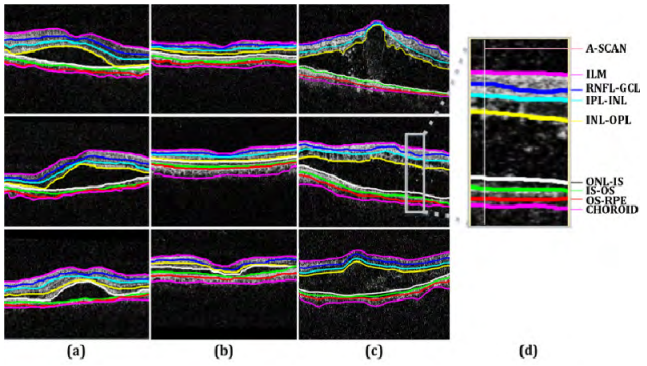

FIGURE 4. Segmented retinal layers (a) CSCR affected frame, (b) healthy frame, (c) ME affected frame, (d) segmented retinal layers in one A-scan: ILM, RNFL-GCL, IPL- INL, INL- OPL, ONL- IS, IS-OS, OS-RPE and choroid.

It can be observed from Figure 4 that in case of healthy subjects, all retinal layers are closely intact whereas in case of CSCR and ME, retinal layers are detached due to fluid spaces in between them. Table 2 shows the axial scans (A-scans) mean separation between retinal layers of all 3 types of retinal

TABLE 2. Retinal and choroidal layers separation for all 3 types of retinal subjects.

Layers	Healthy	CSCR	ME
	Mean ± S.D (μm)	Mean ± S.D (μm)	Mean ± S.D (μm)
ILM-RNFL	36.789 ± 6.2	67.248 ± 10.29	84.215 ± 14.71
RNFL-INL	38.114 ± 5.4	54.764 ± 13.17	124.10 ± 16.68
INL-OPL	40.028 ± 8.1	42.857± 8.76	115.738 ± 15.92
OPL-ONL	32.582 ± 5.8	248.168 ± 32.64	201.612 ± 24.09
ONL-OS	31.937 ± 4.8	74.599 ± 15.85	192.577 ± 21.96
OS-RPE	32.743 ± 2.7	60.008 ± 15.08	108.349 ± 14.79
RPE-CHOROID	31.327 ± 9.2	64.386 ± 9.78	96.47± 17.63

disorders. It can be observed from the tabulated data that in case of healthy subjects, mean value for all retinal layers is less as compared to CSCR and ME cases.

C. MACULAR FLUIDS EXTRACTION

After segmenting retinal layers, ILM and RPE are used to automatically extract fluid segments by creating a retinal mask $F_{Mask}(x, y)$. F_{Mask} (x, y) is a binary map that is created by keeping all the pixels in between ILM and RPE as 1's and rest of the pixels as 0's. After creating a mask, it is multiplied with F (x, y) to extract neurosensory retina F_N (x, y) as expressed in Eq. (1).

$$F_N(x, y) = F_{Mask}(x, y) \times F(x, y) \tag{1}$$

After extracting F_N (x, y), the macular fluids are automatically obtained by digitalizing F_N (x, y) through Otsu's threshold. Figure 5 shows the extracted fluid segment for the randomly selected scan.

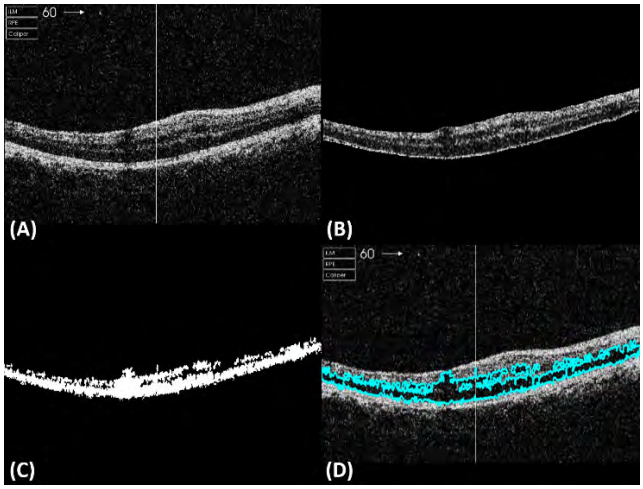

FIGURE 5. Macular fluid extraction: (A) original retinal OCT scan F (x, y), (B) neurosensory retina F_N (x, y), (C) binary map of auto-extracted fluid (D) fluid mapped on F (x, y).

The proposed system is extremely robust in extracting fluid segments while preserving the retinal portion as it is evident from Figure 6, where due to the presence of fluid, some of the retinal portions are isolated. However, the proposed system efficiently discriminates those portions from the fluid affected area.

D. 3D ANALYSIS

After extracting the retinal and choroidal layers, the proposed system generates the B-scan thickness profile by taking the absolute difference between extracted ILM and RPE layers. This process is repeated for all the B-scans within OCT volume $V_{OCT}(x, y, z)$, yielding a retinal thickness map $T \epsilon \mathbb{R}^{M \times N}$ as expressed below:

$$T = \sum_{i=0}^{K-1} \sum_{j=0}^{T_A-1} |RPE_j^i - ILM_j^i| \tag{2}$$

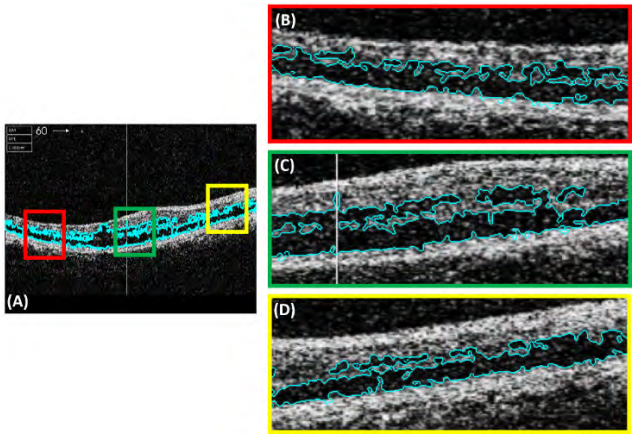

FIGURE 6. Detailed visualization of extracted fluid: (A) scan with extracted fluid at original zoom level, (B) 3 times zoomed portion under red rectangle in A, (C) 3 times zoomed portion under green rectangle in A (D) 3 times zoomed portion under yellow rectangle in A.

where M denotes the height of the map, N denotes the width of the map, K denotes the total frames within $V_{OCT}(x, y, z)$ and it is equal to 128 in AFIO dataset as described in Table 1, T_A denotes the total number of A-scans within each B-scan and it is equal to 951 in AFIO dataset as shown in Table 1. After generating T, its spatial coordinates along with its intensities are used to reconstruct 3D retinal surfaces which depicts the objective visualization of maculopathy. In [19], we also reconstructed the retinal surfaces for the healthy, ME and CSCR subjects. However in the proposed system, we significantly improved the reconstruction of 3D retinal surfaces as compared to [19] as demonstrated in the result section. Figure 7 shows the reconstructed 3D retinal surface of a randomly selected CSCR subject from AFIO dataset.

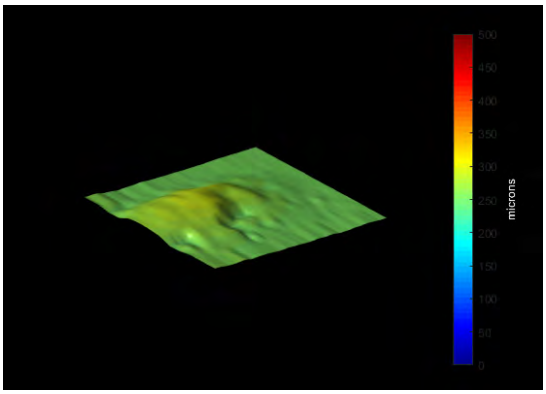

FIGURE 7. Reconstructed 3D retinal thickness surface of a randomly selected Type-II CSCR affected subject.

The level of detailing especially in the thickening region can be easily observed in Figure 7. This high-resolution reconstruction was achieved by decomposing the retinal surface into a 3D polygon ρ_{3D} where the surface normal at each vertex of a polygon is computed by taking an average of the cross product between its tangent vectors. After computing

TABLE 3. Feature set description for maculopathy diagnosis.

Category	Feature	Description	Mathematical Expression
2D	**Maximum Thickness**	It is the peak point in the thickness map T, which represents the highest absolute difference between ILM and choroid as expressed in Eq. (3) and (4)	$f_1 = \max[\,T_{mn}]$ (3) $f_1 = \max[\lvert B_{ILM}(m,n) - B_{Choroid}(m,n)\rvert]$ (4) where $m = 0, 1, 2, \ldots, M-1$ and $n = 0, 1, 2, \ldots, N-1$
	Minimum Thickness	It is the shallowest point in the thickness map T, which represents the lowest absolute difference between ILM and choroid as expressed in Eq. (5) and (6)	$f_2 = \min[\,T_{mn}]$ (5) $f_2 = \min[\lvert B_{ILM}(m,n) - B_{Choroid}(m,n)\rvert]$ (6) where $m = 0, 1, 2, \ldots, M-1$ and $n = 0, 1, 2, \ldots, N-1$
	Absolute Thickness Variation	It depicts the variation within the macular profile due to the presence of fluid spaces and mathematically this variation is computed using Eq. (7)	$f_3 = \lvert f_2 - f_1\rvert$ (7)
3D	**Fluid Volume**	This feature determines the total fluid volume within the macular region. It is computed by summing the fluid area of all the B-scans within OCT volume as expressed in Eq. (8)	$f_4 = \sum_{i=0}^{K-1} \text{Area}\left(F_N^i(x,y)\right)$ (8)
	Fluid Boundaries Magnitude	This feature describes the strength of change in the fluid boundaries and it is computed using Eq. (9)	$f_5 = \text{mean}\left(\sum_{i=0}^{K-1}\sqrt{\left(\frac{\partial F_N^i(x,y)}{\partial x}\right)^2 + \left(\frac{\partial F_N^i(x,y)}{\partial y}\right)^2}\right)$ (9)
	Mean of Fluid Orientation	This feature describes the orientation of fluid change and it is calculated using Eq. (10)	$f_6 = \text{mean}\left(\sum_{i=0}^{K-1}\tan^{-1}\left(\frac{\frac{\partial F_N^i(x,y)}{\partial y}}{\frac{\partial F_N^i(x,y)}{\partial x}}\right)\right)$ (10)
	Fluid Segments Count	It is the total count of fluid segments present within macular region as expressed in Eq. (11)	$f_7 = \sum_{i=0}^{K-1}\sum_{k=1}^{\gamma}\left(F_N^{i,k}(x,y)\right)$ (11) where γ denotes total fluid segments with a single B-scan

the surface normal, their intensities at each vertex is computed through Phong reflection model [25] that computes the intensities at each vertex 'v' through:

$$I_v = k_a i_a + \sum_{m=0}^{N_l} \left(k_d\,(L_m.\aleph)\,i_{m,d} + k_s\,(R_m.V)^{\alpha}\,i_{m,s}\right) \quad (12)$$

where R_m is a directional vector and it is calculated as:

$$R_m = 2\,(L_m.\aleph)\,N - L_m \quad (13)$$

I_v denotes the calculated intensity at vertex v, L_m is the directional vector from v to the light source m, $\aleph$ denotes the surface normal at v, V is the directional vector pointing towards the camera, N_l is the total number of light sources, $i_{m,d}$ and $i_{m,s}$ defines the intensity of diffuse and specular component of the m^{th} light source respectively, k_a is the ambient reflection constant, k_s is the specular reflection constant, k_d is the diffuse reflection constant, α is the shinning constant, i_a is the intensity of the ambient lightning, i_s is the specular lightning intensity and i_d is the intensity of diffuse lightning component where i_a, i_d and i_s are initialized through the color intensities of retinal thickness surface. The dot symbol '.' denotes the dot product and all the vectors in Eq. (12) and (13) are normalized.

Apart from extracting 3D retinal surfaces, the proposed system also generates the fluid volume by stacking all the fluid scans within an OCT volume. These fluid B-scans are further utilized in grading the maculopathy.

E. MACULOPATHY CLASSIFICATION AND GRADING

1) MACULOPATHY CLASSIFICATION

After generating the 3D retinal information from the candidate OCT volume, the proposed system utilizes it to diagnose as well as grade the underlying retinal condition. The proposed system utilizes hierarchical SVM based classification model which first categorizes the candidate subject as healthy or diseased through the set of discriminating features, extracted from the retinal information. If the candidate is diagnosed as diseased then the proposed system categorizes the subject as ME or CSCR. Furthermore, the diagnosed maculopathy is automatically graded as per clinical standards by the proposed system. To the best of our knowledge, the proposed system is first of its kind in grading the severity of ME and CSCR syndromes as per CSME, non-CSME, Type-I and Type-II clinical standards. First of all, the proposed system utilizes retinal thickness map T and the fluid volume to generate set of 2D and 3D features as shown in Table 3.

TABLE 4. Retinal layers separation for healthy and maculopathy subjects.

Pathology	Subjects	Features						
		f_1 (mm)	f_2 (mm)	f_3 (mm)	f_4	f_5	f_6	f_7
Healthy	Subject 1	36.51	11.38	25.14	124.27	0.0024	$1.39e^{-6}$	7
	Subject 2	39.69	23.02	16.67	140.28	0.0019	$1.78e^{-6}$	2
	Subject 3	34.13	19.58	14.55	0.00	0	0	0
	Subject 4	50.54	32.54	17.99	126.71	0.0068	$1.41e^{-6}$	4
	Subject 5	38.36	18.26	20.11	174.34	0.012	$1.55e^{-6}$	1
	Mean	**39.84**	**20.95**	**18.89**	**113.12**	**0.0046**	$\mathbf{1.22e^{-6}}$	**2.80**
	S.D	**6.33**	**7.73**	**4.03**	**66.31**	**0.0048**	$\mathbf{7.02e^{-7}}$	**2.77**
CSCR	Subject 1	64.29	38.10	26.19	11827.1	0.0096	$7.18e^{-6}$	15
	Subject 2	82.02	42.33	39.69	20981.4	0.0091	$9.31e^{-6}$	27
	Subject 3	68.79	34.66	34.13	22936.9	0.0064	$9.87e^{-6}$	21
	Subject 4	63.50	43.39	20.11	8724.10	0.0085	$6.92e^{-6}$	16
	Subject 5	71.70	35.98	35.72	26443.2	0.0077	$9.98e^{-6}$	19
	Mean	**70.06**	**38.89**	**31.16**	**18183.0**	**0.0083**	$\mathbf{8.65e^{-6}}$	**19.60**
	S.D	**7.47**	**3.84**	**7.89**	**7558.6**	**0.0013**	$\mathbf{1.48e^{-6}}$	**4.77**
ME	Subject 1	72.23	36.25	35.98	7023.88	0.0058	$1.26e^{-5}$	38
	Subject 2	48.42	25.66	22.75	18400.9	0.0068	$3.56e^{-6}$	42
	Subject 3	49.48	21.96	27.52	14619.3	0.0062	$3.74e^{-6}$	37
	Subject 4	62.18	33.07	29.10	27120.8	0.0076	$1.32e^{-5}$	29
	Subject 5	65.62	39.42	26.19	5201.17	0.0051	$2.72e^{-6}$	42
	Mean	**59.58**	**31.27**	**28.30**	**14473.0**	**0.0063**	$\mathbf{7.16e^{-6}}$	**37.6**
	S.D	**10.36**	**7.29**	**4.88**	**8900.5**	**0.0009**	$\mathbf{5.25e^{-6}}$	**5.31**

First four features are used to diagnose the candidate subject as healthy and diseased through hierarchical SVM model. If the candidate subject is diagnosed as having maculopathy then the proposed system uses the remaining three features for categorizing ME or CSCR.

Table 4 shows some of the features extracted from 5 randomly selected subjects of each type along with the mean and standard deviation value of entire dataset. It can be observed from Table 4 that all 7 features deviated more in case of randomly selected diseased subject 1, 2, 3, 4 and 5 as compared to healthy subjects. This is due to increased fluid density across volumetric scans of ME and CSCR affected eyes.

In order to classify the candidate subject as healthy or diseased, the first four extracted features f_1, f_2, f_3, f_4 are passed to the first stage of SVM classification model. If the candidate subject is classified as diseased then the second stage of SVM classification model classifies the subject as having ME or CSCR through the remaining set of extracted features f_5, f_6, f_7. The reason for using SVM based classification model is because it is fast [26] and it has high performance for binary classification tasks. Also, the SVM employed in the proposed classification system uses the cascade of multilayer perceptron (MLP) and Gaussian Radial Basis Function (RBF) kernel and it is hierarchical which means that at first it is used to diagnose candidate scan as healthy or diseased. If it is diagnosed as diseased then it is further classified as ME or CSCR. The classification model in the proposed system was trained on the set of 30 labeled OCT volumes and it is validated on 90 volumes. The performance of the classification model in training phase was measured using k-fold cross validation where the value of 'k' was iterated from 2 to 12 in step of 2. The maximum accuracy is achieved for k equals to 10 as shown in Table 5 and the respective trained model is chosen for classification.

After training the classification model, it was used to diagnose the random retinal subjects. For diagnosing the test candidate(s), same features are extracted from their retinal information and a diagnosis is made by the proposed system that whether the subject is healthy, ME or CSCR positive. The performance of the classification model is measured through accuracy, sensitivity and specificity ratings which are

TABLE 5. Performance of proposed framework.

Stage	k	Max Accuracy	
Maculopathy Diagnosis	2	0.942	Classification Model
	4	0.957	
	8	0.968	
	10	**0.980**	
	12	0.974	
Maculopathy Characterization	2	0.932	Classification Model
	4	0.957	
	8	0.978	
	10	**0.991**	
	12	0.987	

computed through true positives (TP), false positives (FP), true negatives (TN), and false negatives (FN) as expressed in Eq. (14) to (16):

$$\text{Accuracy} = \frac{\text{TP} + \text{TN}}{\text{TP} + \text{TN} + \text{FP} + \text{FN}} \tag{14}$$

$$\text{Sensitivity} = \frac{\text{TP}}{\text{TP} + \text{FN}} \tag{15}$$

$$\text{Specificity} = \frac{\text{TN}}{\text{TN} + \text{FP}} \tag{16}$$

2) MACULOPATHY GRADING

Apart from diagnosing the maculopathy, the proposed system grades it according to the clinical standards. Clinically, the presence of retinal thickening within the diameter of 500 microns centered at fovea is considered as severe and therefore it is graded as CSME [1]. However, the symptoms of ME outside this limit are graded as non-CSME. For CSCR, if the serous accumulates under the neurosensory retina but above the RPE, then it is graded as Type I CSCR. However, if the serous is formed beneath RPE then it is graded as Type II CSCR [2]. If the candidate subject is diagnosed as ME positive then foveal B-scans of the respective subject are automatically analyzed within the diameter of 500 microns centered at foveal location. If there is a presence of fluid segments within the region in any of the scan then the ME is further graded as CSME. If the proposed system is unable to find the fluid segments within the region then the patient is graded as having non-CSME. Similarly, if the patient is diagnosed as having CSCR then the proposed system localizes serous fluid with respect to extracted RPE. If the majority of serous fluid is found to be beneath the RPE then the diagnosed CSCR is further graded as Type-I. Otherwise if the majority of serous fluid is found to be in between neurosensory retina and RPE then the CSCR is graded as Type-II. Figure 8 shows some of the randomly selected ME and CSCR affected B-scans that are further graded as per clinical standards.

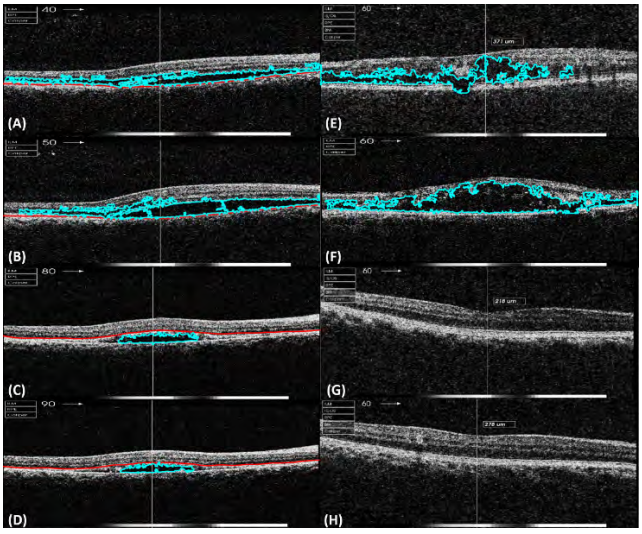

FIGURE 8. Maculopathy grading: (A-B) Type-I CSCR with serous fluid beneath RPE, (C-D) Type-II CSCR with serous fluid in between neurosensory retina and RPE, (E-F) CSME with cyst fluid within B-scan near fovea, (G-H) non-CSME with no cyst fluid within B-scan near fovea.

Apart from this, the complete flow diagram of the proposed system for the classification as well as grading of maculopathy is shown in Figure 9 and Table 6 shows the description of the dataset which has been graded as per clinical standards by multiple expert ophthalmologists. The proposed system is highly sensitive in picking small retinal variations which are fully utilized in grading the maculopathy. Furthermore, all those retinal variations can be clearly observed on the reconstructed 3D retinal surfaces as well.

TABLE 6. Grading description (the grading information is also described in Table 1 as well).

ME			CSCR		
Total	CSME	Non-CSME	Total	Type 1	Type 2
40	23	17	40	31	9

Figure 10 shows some of the graded B-scans along with the corresponding reconstructed surfaces. It can be observed from Figure 10 that the proposed system presents a highly detailed representation of 3D retinal thickness. Furthermore, all the pathological variations of maculopathy can also be clearly visualized.

III. RESULTS

The proposed system was tested on the dataset that is acquired in AFIO, Rawalpindi Pakistan and it has been validated by multiple expert ophthalmologists. The dataset has overall

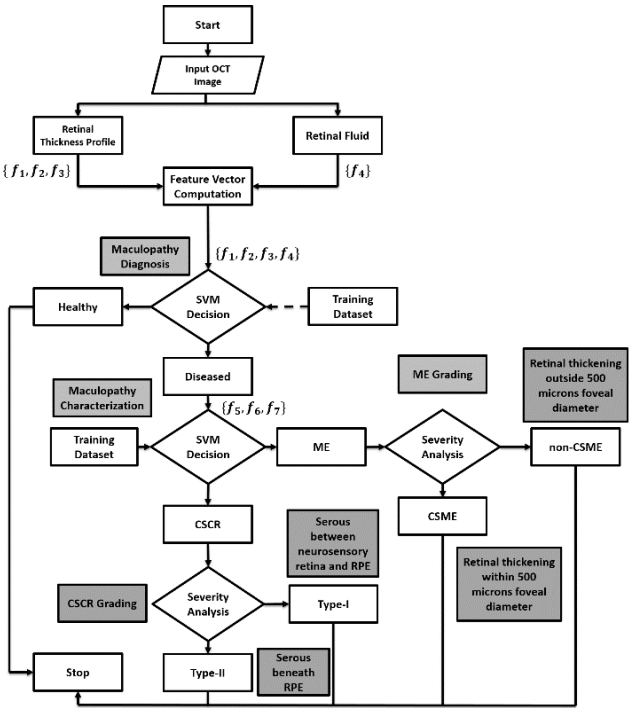

FIGURE 9. Flowchart of classification algorithm.

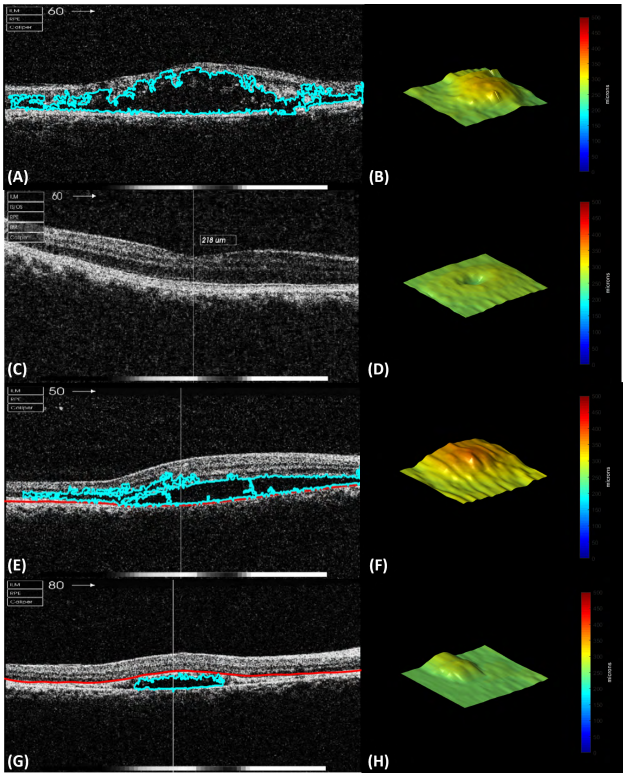

FIGURE 10. Graded 3D retinal surfaces (A) CSME graded B-scan, (B) 3D retinal surface of a CSME subject, (C) non-CSME graded B-scan, (D) 3D retinal surface of a non-CSME subject, (E) Type-I CSCR graded B-scan, (F) 3D retinal surface of a Type-I CSCR subject, (G) Type-II CSCR graded B-scan, (H) 3D retinal surface of a Type-II CSCR subject.

120 OCT volumes from which 30 are used for training the classification model, while 90 are used for validating the proposed system. Out of those 90 volumes, 30 scans depict healthy pathology, 30 scans are of ME and the remaining 30 scans show the CSCR pathology. The proposed system was able to correctly predict all the diseased scans and 28/30 healthy scans. All the predictions have been cross validated by expert ophthalmologists and Table 7 shows the overall performance of the proposed system.

TABLE 7. Performance on validation set.

Type	Correctly Classified	Specificity	Sensitivity	Accuracy
ME	30 / 30			
CSCR	30 / 30	100%	96.77%	97.78%
Healthy	28 / 30			

Furthermore, the ST-GS framework has been validated against manual annotations for different retinal pathologies by measuring the mean error rate. Mean error rates are computed by taking the absolute difference of ST-GS segmented layers from manual annotations and then taking their mean. Table 8 shows the mean retinal layers segmentation error from five randomly selected samples of each category. Moreover,

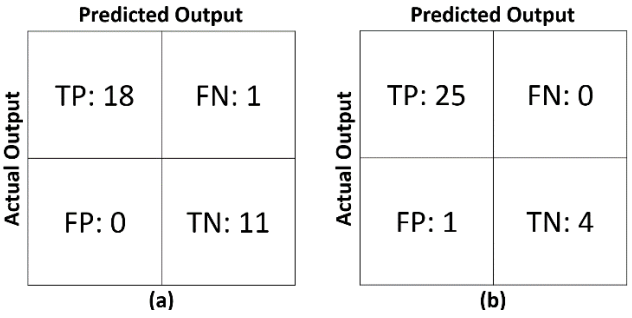

FIGURE 11. Confusion matrices showing the performance of (a) ME grading as CSME and non-CSME, (b) CSCR grading as Type-I and Type-II.

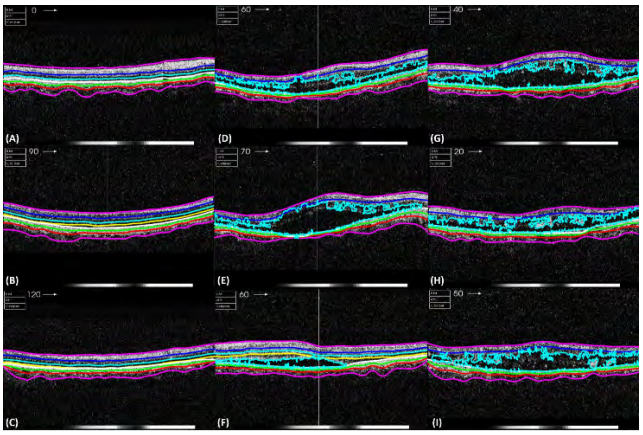

FIGURE 12. Extracted retinal and choroidal layers along with maculopathy from (A-C) healthy B-scans, (D-F) CSCR affected B-scans, (G-I) ME affected scans.

TABLE 8. Mean retinal layers segmentation error.

Layers	ILM	RNFL-GCL	IPL-INL	OPL	ONL	IS-OS	RPE	Choroid
	0.0045	0.0110	0.0328	0.0211	0.0820	0.0455	0.0954	0.0990
	0.0594	0.0498	0.0103	0.0268	0.0639	0.0096	0.0707	0.0838
CSCR	0.0559	0.0397	0.0014	0.0218	0.0836	0.0291	0.0904	0.1039
	0.0541	0.0461	0.0174	0.0295	0.0198	0.0102	0.0226	0.0310
	0.0460	0.0352	0.0050	0.0092	0.0543	0.0145	0.0597	0.0733
Mean	**0.0440**	**0.0364**	**0.0134**	**0.0217**	**0.0607**	**0.0218**	**0.0678**	**0.0782**
S.D	**0.0202**	**0.0136**	**0.0110**	**0.0069**	**0.0232**	**0.0137**	**0.0260**	**0.0259**
	0.0102	0.0111	0.0125	0.0269	0.0414	0.1352	0.0756	0.0725
	0.0122	0.0151	0.0075	0.0432	0.0245	0.1215	0.0614	0.0615
ME	0.0247	0.0203	0.0113	0.0492	0.0387	0.1580	0.0662	0.0632
	0.0518	0.0400	0.0561	0.0664	0.0605	0.1469	0.0861	0.0736
	0.0102	0.0111	0.0125	0.0269	0.0414	0.1352	0.0756	0.0725
Mean	**0.0247**	**0.0216**	**0.0218**	**0.0465**	**0.0413**	**0.1404**	**0.0723**	**0.0677**
S.D	**0.0166**	**0.0111**	**0.0199**	**0.0141**	**0.0128**	**0.0136**	**0.0095**	**0.0054**
	0.0500	0.0526	0.1764	0.0294	0.0361	0.4056	0.1552	0.1102
	0.0479	0.0219	0.1759	0.0264	0.0428	0.4134	0.1816	0.1609
Healthy	0.0546	0.0614	0.2427	0.0760	0.0391	0.4325	0.1695	0.1416
	0.0443	0.0237	0.2003	0.0177	0.0110	0.1413	0.1729	0.1522
	0.0555	0.0392	0.1874	0.0082	0.0336	0.4041	0.1260	0.1024
Mean	**0.0505**	**0.0398**	**0.1965**	**0.0315**	**0.0325**	**0.3594**	**0.1610**	**0.1335**
S.D	**0.0042**	**0.0156**	**0.0247**	**0.0234**	**0.0112**	**0.1095**	**0.0195**	**0.0231**

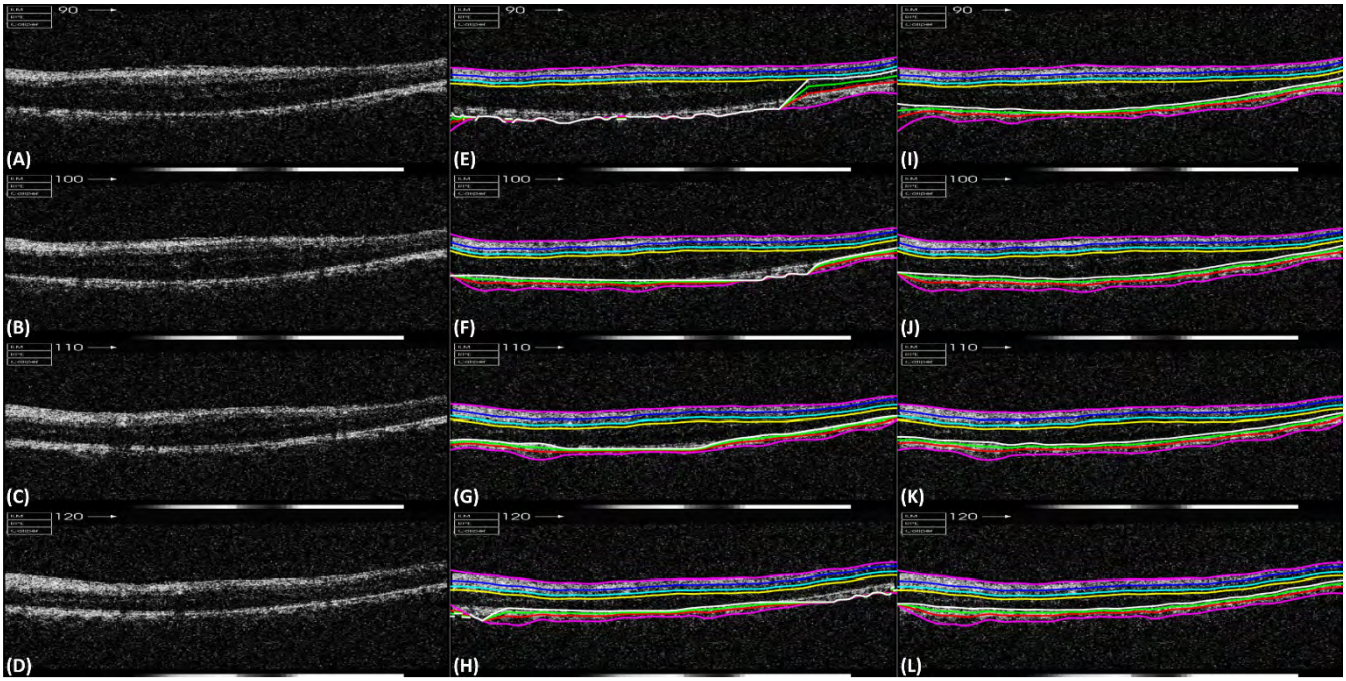

FIGURE 13. Comparison of retinal and choroidal layers extraction: (A-D) original ME affected B-scans, (E-H) layers extraction through segmentation framework used in [20]–[22], (I-L) layers extracted through the proposed ST-GS framework.

the performance of the proposed system to automatically grade maculopathy on the validation set is depicted by the confusion matrices in Figure 11.

Figure 12 shows some of the randomly selected B-scans healthy, CSCR and ME subjects. The extracted fluid is represented by the cyan color while the retinal layers follow the color scheme as shown in Figure 4. The robustness of proposed ST-GS framework can be easily seen from Figure 12 where ST-GS is able to extract up to eight retinal and choroidal layers from scans showing different retinal pathological conditions. Moreover, the proposed system is able to automatically extract macular fluids with high precision as evident from Figure 12.

Apart from this, the proposed system utilizes the extracted retinal information to reconstruct 3D retinal thickness surfaces. Previously we proposed an automated framework to

reconstruct 3D retinal surfaces [19]. However, this paper presents a significantly improved 3D representation of retinal thicknesses. The comparison of the proposed system with [19] is presented in Figure 14.

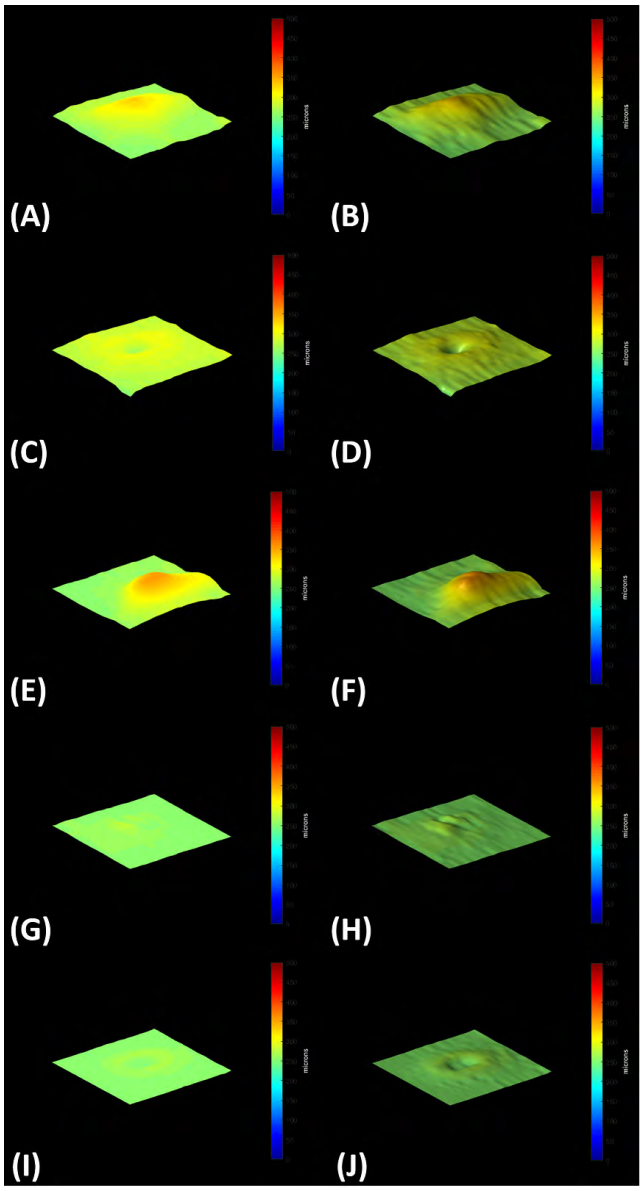

FIGURE 14. Comparison of 3D retinal surface reconstruction: (A) reconstructed surface of a CSME subject using [19], (B) reconstructed surface of a CSME subject through the proposed system, (C) reconstructed surface of a non-CSME subject using [19], (D) reconstructed surface of a non-CSME subject through the proposed system, (E) reconstructed surface of a Type-I CSCR subject using [19], (F) reconstructed surface of a CSME subject through the proposed system, (G) reconstructed surface of a Type-II CSCR subject using [19], (H) reconstructed surface of a Type-II CSCR subject through the proposed system, (I) reconstructed surface of a healthy subject using [19], (J) reconstructed surface of a healthy subject through the proposed system. Please note here that the method proposed in [19] only reconstructs retinal surfaces irrespective of disease grading.

The extraction of macular fluids by the proposed system has been validated by measuring the dice coefficient between the auto-extracted fluid and the fluid annotations which were performed by expert ophthalmologists. Dice coefficient is computed through [27]:

$$DC = \frac{2|X \cap Y|}{|X| + |Y|} \tag{17}$$

where DC represents the dice coefficient, X denotes the auto-extracted fluid maps and Y denotes the fluid annotations marked by the expert ophthalmologists. The fluid markings have been made in AFIO dataset by two expert ophthalmologists based on their own experience and without any assistance. Those markings were the ground truth to validate the fluid extraction of the proposed system. Table 9 shows the dice coefficient on 10 randomly selected maculopathy subjects (5 ME and 5 CSCR) having different severity levels. These dice coefficients are computed using the fluid annotations marked by both ophthalmologists. As evident from Table 9, the fluid extraction by the

TABLE 9. Dice coefficient ratings for macular fluids extraction.

Disease	Grading	Ophthalmologist 1	Ophthalmologist 2
ME	CSME	0.90	0.92
	CSME	0.88	0.90
	CSME	0.91	0.90
	non-CSME	0.83	0.85
	non-CSME	0.85	0.84
	Mean ± STD	**0.87 ± 0.0336**	**0.88 ± 0.0349**
CSCR	Type-I	0.91	0.92
	Type-I	0.93	0.95
	Type-II	0.94	0.96
	Type-II	0.87	0.89
	Type-II	0.92	0.93
Mean ± STD		**0.91 ± 0.0270**	**0.93 ± 0.0247**

proposed system is extremely robust where the proposed system achieved a mean dice coefficient of 0.875±0.0342 in between both markings of ME subjects and a mean dice coefficient of 0.92±0.0258 for extracting serous fluid from CSCR affected subjects.

The proposed system has been thoroughly compared with our previous work [19]–[22], where the proposed system produces better results in extracting retinal and choroidal layers, macular fluids and reconstructing 3D retinal thickness surfaces. The retinal layers extraction through our previous framework had a limitation on the quality of acquired scan however the proposed ST-GS framework can automatically extract retinal and choroidal layers irrespective of the scan quality. This is accomplished through efficient graph searches which are sensitive to even small retinal variations and due to which the low intensity components of retinal layers are automatically traced. Figure 13 shows some of the ME affected scans on which our previous segmentation framework did not perform well, whereas ST-GS is able to efficiently capture the retinal and choroidal layers information.

Furthermore, the reconstruction of 3D retinal surfaces by the proposed system is also compared with [19] where the proposed system outperformed [19] by providing high resolution details and presentation of retinal anomalies as compared to [19]. Figure 14 shows some of the 3D retinal thickness surfaces from normal as well as maculopathy affected subjects, where it can be observed that the proposed system provide significantly better presentation of retinal thickening due to presence of macular fluids as compared to [19]. It is also worth noting that the method proposed in [19] only reconstructs the retinal surfaces irrespective of the knowledge about their grading on clinical standards, whereas the proposed system efficiently reconstructs 3D retinal surfaces which reflects highly detailed retinal variations under different disease severity levels as shown in Figure 14.

IV. DISCUSSION

We have proposed an automated system that can be used for the automated diagnosis and grading of ME, CSCR and healthy pathology from OCT volumetric scans. ME and CSCR are the macular disorders which are frequently associated with diabetes. These disorders mostly affect the young generation between 30-50 years. OCT is an eye testing technique which provides an objective evaluation of retinal pathology. Symptoms of retinal diseases appear at early stages in OCT scans. It is also possible to estimate the severity of retinal disorders from OCT imagery. The proposed system is based on novel ST-GS framework to extract up to eight retinal layers and the macular fluid pathology followed by the robust reconstruction of 3D retinal profiles from OCT scans. To the best of our knowledge, the proposed system is first of its kind that provides fully automated diagnosis of ME and CSCR pathologies along with their severity analysis and grading as per clinical standards. Moreover, the performance of the proposed system is remarkable as shown in Table 7. The automated grading and 3D profiling of maculopathy takes one minute on average using 4th generation core i7 (1.8 GHz) processor with 8 GB RAM. The proposed system was tested on local dataset acquired in AFIO Rawalpindi, where the proposed method correctly classified all of ME and CSCR volumes. Previously, we have reported retinal and choroidal layers segmentation framework in [20]–[22], however they had a limitation on the quality of the scan for accurate segmentation. ST-GS framework proposed in this paper can efficiently extract up to eight retinal and choroidal layers from the scans irrespective of their acquisition quality or the type of pathology they depict. This is clearly evident from Figure 13.

Furthermore, the proposed system has been randomly tested on different scans depicting different retinal pathology where the proposed system efficiently extracts the retinal information which leads towards objective grading and 3D visualization of retinal pathology. The proposed system also acts as an aid to ophthalmologists to mass screen retinal patients across different geographical areas of the world. Auto-generated 3D profiles and maculopathy grading reports from the proposed system can also support the diagnosis of ophthalmologists through quantitative numbers and standardize measurements.

V. CONCLUSION

We have presented a novel OCT based clinical decision support system that can diagnose and grade ME and CSCR. The proposed method relies on the robust generation of 3D retinal profiles and retinal fluid through ST-GS based segmentation framework. Apart from this, the proposed system utilizes hierarchical SVM classification model for the diagnosis of normal, ME and CSCR subjects. The diseased candidates are further graded based upon the disease severity level. The proposed system is randomly tested on the validation set consisting of 90 OCT volumes, out of which 60 are diseased (30 ME affected volumes and 30 CSCR affected volumes) and the remaining 30 depicts healthy pathology. The dataset has been annotated by multiple ophthalmologists. The classification in the proposed framework is done by extracting different 2D and 3D features from each candidate OCT volume and then passing it to the hierarchical SVM based classification system. After that the proposed system automatically measures the severity of the disease by grading it according to clinical standards. Currently we have applied this system for the automated diagnosis and severity analysis of ME and CSCR. However, it can be used for the grading and 3D profiling of other retinal diseases as well.

ACKNOWLEDGMENT

This work is funded by Ignite National Technology Fund, Government of Pakistan. We are also thankful to AFIO, Rawalpindi Pakistan for providing us the dataset to conduct this research.

REFERENCES

[1] L. Conceicao, I. Pires, and J. C. Vaz, "Diabetic macular edema," in *Optical Coherence Tomography: A Clinical and Technical Update*, 1st ed. Berlin, Germany: Springer-Verlag, 2012, pp. 1–21.

[2] N. Vukojevic, J. Sikic, D. Katusic, and B. Saric, "Types of central serous retinopathy, analysis of shape, topographic distribution and number of leakage sites," *Collegium Antropologicum*, vol. 25, no. 1, pp. 83–87, Jun. 2001.
[3] T. Hassan, M. U. Akram, B. Hassan, A. Nasim, and S. A. Bazaz, "Review of OCT and fundus images for detection of macular edema," in *Proc. IEEE 12th Int. Conf. Imag. Syst.*, Sep. 2015, pp. 1–4.
[4] R. Z. Hannouche and M. P. Ávila, "Detection of diabetic foveal edema with biomicroscopy, fluorescein angiography and optical coherence tomography," *Arquivos Brasileiros Oftalmologia*, vol. 71, no. 5, pp. 759–763, Oct. 2008.
[5] W. Zhang, K. Yamamoto, and S. Hori, "Optical coherence tomography for assessment of diabetic macular edema," *Int. J. Ophthalmol.*, vol. 1, no. 4, pp. 370–373, Sep. 2008.
[6] A. Shrestha, N. Maharjan, A. Shrestha, R. Thapa, and G. Poudyal, "Optical coherence tomographic assessment of macular thickness and morphological patterns in diabetic macular edema: Prognosis after modified grid photocoagulation," *Nepal J. Ophthalmol.*, vol. 4, no. 7, pp. 128–133, Feb. 2012.
[7] N. F. Mokwa, T. Ristau, P. A. Keane, B. Kirchhoff, S. R. Sadda, and S. Liakopoulos, "Grading of age-related macular degeneration: Comparison between color fundus photography, fluorescein angiography, and spectral domain optical coherence tomography," *J. Ophthalmol.*, vol. 2013, pp. 1–6, Apr. 2013.
[8] Y. M. Helmy and H. R. A. Allah, "Optical coherence tomography classification of diabetic cystoid macular edema," in *Clinical Ophthalmology*. Auckland, New Zealand: Dove Press, Aug. 2013, no. 7, pp. 1731–1737.
[9] D. Ferrara *et al.*, "En face enhanced-depth swept-source optical coherence tomography features of chronic central serous chorioretinopathy," *Amer. Acad. Ophthalmol.*, vol. 121, no. 3, pp. 719–726, Mar. 2014.
[10] J. S. Wani, P. A. Bhat, A. Ahangar, and S. Ismail, "Role of optical coherence tomography in central serous chorioretinopathy," *J. Evol. Med. Dental Sci.*, vol. 4, no. 45, pp. 7801–7809, Jun. 2015.
[11] M. Y. Teke, U. Elgin, P. N. Yuksekkaya, E. Sen, P. Ozdal, and F. Ozturk, "Comparison of autofluorescence and optical coherence tomography findings in acute and chronic central serous chorioretinopathy," *Int J. Ophthalmol.*, vol. 7, no. 2, pp. 350–354, Apr. 2014.
[12] C. Ahlers, W. Geitzenauer, G. Stock, I. Golbaz, U. S. Erfurth, and C. Prunte, "Alterations of intraretinal layers in acute central serous chorioretinopathy," *Acta Ophthalmol.*, vol. 87, no. 5, pp. 511–516, Aug. 2009.
[13] K. Mitarai, F. Gomi, and Y. Tano, "Three-dimensional optical coherence tomographic findings in central serous chorioretinopathy," *Graefe's Arch Clin. Exp. Ophthalmol.*, vol. 244, no. 11, pp. 1415–1420, Nov. 2006.
[14] G. R. Wilkins, O. M. Houghton, and A. L. Oldenburg, "Automated segmentation of intraretinal cystoid fluid in optical coherence tomography," *IEEE Trans. Biomed. Eng.*, vol. 59, no. 4, pp. 1109–1114, Apr. 2012.
[15] J. Sugruk, S. Kiattisin, and A. L. Lasantitham, "Automated classification between age-related macular degeneration and diabetic macular edema in OCT image using image segmentation," in *Proc. IEEE Biomed. Eng. Int. Conf.*, Nov. 2014, pp. 1–4.
[16] L. Zhang, W. Zhu, F. Shi, H. Chen, and X. Chen, "Automated segmentation of intraretinal cystoid macular edema for retinal 3D OCT images with macular hole," in *Proc. Int. Symp. Biomed. Imag.*, Apr. 2015.
[17] P. P. Srinivasan *et al.*, "Fully automated detection of diabetic macular edema and dry age-related macular degeneration from optical coherence tomography images," *Biomed. Opt. Express*, vol. 5, no. 10, pp. 3568–3577, 2014.
[18] A. Rashno *et al.*, "Fully automated segmentation of fluid/cyst regions in optical coherence tomography images with diabetic macular edema using neutrosophic sets and graph algorithms," *IEEE Trans. Biomed. Imag.*, vol. 65, no. 5, pp. 989–1001, May 2018.
[19] A. M. Syed, T. Hassan, M. U. Akram, S. Naz, and S. Khalid, "Automated diagnosis of macular edema and central serous retinopathy through robust reconstruction of 3D retinal surfaces," *Comput. Methods Programs Biomedicine*, vol. 137, pp. 1–10, Dec. 2016.
[20] S. Khalid, M. U. Akram, T. Hassan, A. Nasim, and A. Jameel, "Fully automated robust system to detect retinal edema, central serous chorioretinopathy, and age related macular degeneration from optical coherence tomography images," *BioMed Res. Int.*, vol. 2017, 2017, Art. no. 7148245, doi: 10.1155/2017/7148245.
[21] B. Hassan, G. Raja, T. Hassan, and M. U. Akram, "Structure tensor based automated detection of macular edema and central serous retinopathy using optical coherence tomography images," *J. Opt. Soc. Amer. A, Opt. Image Sci.*, vol. 33, no. 4, pp. 455–463, Jan. 2016.
[22] T. Hassan, M. U. Akram, B. Hassan, A. M. Syed, and S. A. Bazaz, "Automated segmentation of subretinal layers for the detection of macular edema," *Appl. Opt.*, vol. 55, no. 3, pp. 454–461, Jan. 2016.
[23] J. S. Lim, "Image restoration," *Two-Dimensional Signal Image Process*, 1st ed. Englewood Cliffs, NJ, USA: Prentice-Hall, 1990, pp. 536–540.
[24] H. Knutsson, "Representing local structure using tensors," in *Proc. 6th Scand. Conf. Image Anal.*, pp. 241–251, 1989.
[25] R.-E. Fan, K.-W. Chang, C.-J. Hsieh, X.-R. Wang, and C.-J. Lin, "LIBLINEAR: A library for large linear classification," *J. Mach. Learn. Res.*, vol. 9, no. 9, pp. 1871–1874, Aug. 2008.
[26] B. T. Phong, "Illumination for computer generated pictures, Communications," *Commun. ACM*, vol. 18, no. 6, pp. 311–317, 1975.
[27] M. Murguia and J. L. Villasenor, "Estimating the effect of the similarity coefficient and the cluster algorithm on biogeographic classifications," *Ann. Botanici Fennici*, vol. 40, no. 6, pp. 415–421, 2003.

TAIMUR HASSAN received the B.S. degree in computer engineering from Bahria University, Islamabad, in 2013, and the M.S. degree in computer engineering from the Center for Advanced Studies in Engineering, University of Engineering and Technology, Taxila, in 2015. He is currently pursuing the Ph.D. degree in computer engineering from the College of Electrical and Mechanical Engineering, National University of Sciences and Technology, Islamabad. His research interests lie in the areas of medical image analysis, machine learning, embedded systems, and wireless communications.

MUHAMMAD USMAN AKRAM (M'09) received the B.S., M.S., and Ph.D. degrees in computer engineering from the College of Electrical and Mechanical Engineering (CE&ME), National University of Sciences and Technology (NUST), Islamabad. He is currently an Associate Professor with the Department of Computer and Software Engineering, CE&ME, NUST. He is also heading the Emerging Technologies Laboratory, Biomedical Image and Signal Analysis research group, CE&ME, NUST. His interest lies in the areas of medical image analysis, biomedical signal processing, machine learning, pattern recognition, and biometrics. He was a recipient of many national and international awards.

ARSLAN SHAUKAT received the B.S. and M.S. degrees in computer engineering and the Ph.D. degree in computer science. He is currently an Assistant Professor with the Department of Computer and Software Engineering, College of Electrical and Mechanical Engineering, National University of Sciences and Technology, Islamabad. His research interests lie in the areas of speech processing, machine learning, deep learning, pattern recognition, and artificial intelligence.

SAJID GUL KHAWAJA received the B.S., M.S., and Ph.D. degrees in computer engineering from the College of Electrical and Mechanical Engineering (CE&ME), National University of Sciences and Technology (NUST), Islamabad. He is currently an Assistant Professor with the Department of Computer and Software Engineering, CE&ME, NUST. His research interests lie in the areas of embedded systems, image processing, and machine learning.

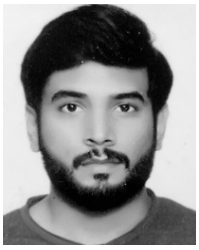

BILAL HASSAN received the B.S. degree in telecommunication engineering from Foundation University, Islamabad, in 2013, and the M.S. degrees in electrical engineering from the University of Engineering and Technology, Taxila, in 2016. He is currently pursuing the Ph.D. degree with the School of Automation Science and Electrical Engineering, Beihang University, Beijing, China. His research interests lie in the areas of image processing, control, and communication systems.